Achieving phase-regulated robust quantum entanglement in cavity magnomechanics

Jing-Xue Liu,[1] Wen-Jing Hu,[1] Baijun Li,[2] Tian-Xiang Lu,[3,*] and Chun-Jie Yang[1,†]

[1]*School of Physics, Henan Normal University, Xinxiang 453007, China*
[2]*Research Center for Quantum Physics, Huzhou University, Huzhou 313000, China*
[3]*College of Physics and Electronic Information, Gannan Normal University, Ganzhou 341000, China*

(Received 3 November 2025; accepted 29 June 2026; published 24 July 2026)

Generating strongly entangled states within multiparticle systems stands as a pivotal endeavor in quantum physics. It not only serves as a cornerstone for delving into the intrinsic properties of quantum mechanics but also provides indispensable quantum resources vital for the development of emerging quantum technologies that transcend classical capabilities. Here, we propose a method to manipulate the magnon-photon, magnon-phonon, and photon-phonon robust entanglement, and the tripartite entanglement involving magnon, photon, and phonon modes, within a hybrid cavity magnomechanical system, leveraging the interference effects induced by two counterpropagating pump lasers. We find that it becomes feasible to exert effective control over all three different types of bipartite quantum entanglement and the tripartite quantum entanglement by properly adjusting the phase difference between the two pump lasers. Moreover, this approach not only enhances these entanglements but also bolsters their resilience against thermal noise emanating from the surrounding environment. The outcomes of our research reveal a readily implementable technique for the manipulation and preservation of quantum entanglement. This technique is of paramount importance in numerous real-world applications that hinge on purely quantum resources, including noise-resistant quantum computing and high-precision quantum measurements.

DOI: 10.1103/j66f-r7w6

I. INTRODUCTION

The hybrid cavity magnomechanical (CMM) system, a composite quantum framework that integrates optical cavity (photon), magnon, and mechanical (phonon) modes, serves as a highly promising platform for exploring a diverse array of intriguing physical phenomena [1–6]. In a hybrid CMM system, the collective spin dynamics—specifically, magnons within the Kittel mode of ferromagnetic crystals such as yttrium-iron-garnet (YIG) spheres—exhibit exceptional experimental versatility and tunability [7–9]. Based on such properties, the hybrid CMM system provides a multifunctional platform with extensive applicability, covering areas such as mechanical cooling processes [10], quantum parametric amplification [11], quantum state manipulation [12–14], the generation of magnonic frequency combs [15–18], and magnomechanical chaos phenomena [19–21]. Notably, quantum entanglement based on CMM [22–27] represents a distinctive quantum resource. In particular, in Ref. [28], it has been proved that optimal parameter regimes for achieving the tripartite entanglement where magnons, cavity photons, and phonons are entangled with each other. Furthermore, in Ref. [29], it has been shown that nonreciprocal modulation of entanglement utilizing the magnon Kerr effect is possible. However, research on phase regulation of bipartite entanglement based on such systems is still lacking. Significantly, quantum entanglement has undergone experimental validation in diverse optical fields [30,31] and mechanical oscillator setups [32–35]. Nonetheless, quantum entanglement usually demonstrates fragility and is easily disturbed by random noise. As a result, in real-world applications, there exists an urgent and critical need to protect and enhance quantum entanglement.

In this paper, we propose a scheme to control and enhance the robust magnon-photon, magnon-phonon, and photon-phonon entanglement, as well as the tripartite entanglement within a hybrid quantum CMM system. This is achieved through the utilization of two pump lasers that travel in different directions. We observe that one-way optical transmission has been achieved experimentally through the adjustment of the phase difference between the two pump lasers, utilizing a whispering-gallery-mode resonator [36,37]. We have also noticed that the relative phase between two microwave tones can be manually set using an arbitrary waveform generator and an in-phase and quadrature mixer, and phase-dependent switching among magnon-induced transparency, absorption, and amplification has been experimentally realized [38]. By employing dual-drive systems, it is also possible to achieve a variety of other quantum effects, including optical nonreciprocity based on a double-cavity optomechanical system [39] or a three-mode optomechanical system [40], phonon lasering based on a cavity magnomechanical system [41], quantum entanglement based on a cavity optomechanics

*Contact author: lu.tianxiang@foxmail.com
†Contact author: yangchunjie@htu.edu.cn

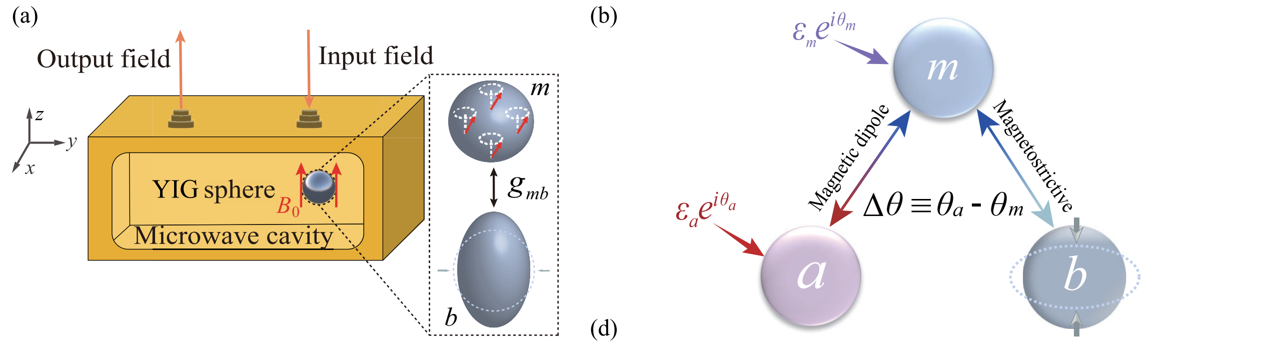

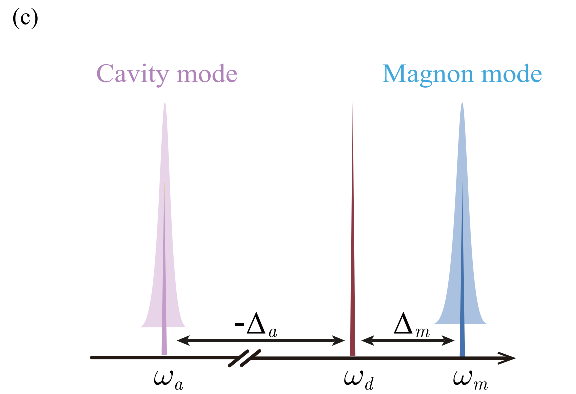

Symbol	Name	Value
$\omega_a/2\pi$	Cavity mode frequency	10 GHz
$\omega_m/2\pi$	Magnon mode frequency	10.1 GHz
$\omega_b/2\pi$	Mechanical mode frequency	10 MHz
$\kappa_a/2\pi$	Cavity decay rate	1 MHz
$\kappa_m/2\pi$	Magnon decay rate	1 MHz
$\gamma_b/2\pi$	Mechanical damping rate	100 Hz
$g_{ma}/2\pi$	Magnon-microwave coupling rate	1 MHz
$g_{mb}/2\pi$	Magnomechanical coupling rate	0.3 Hz
P_a	Input laser power of cavity mode	30 mW
P_m	Input laser power of magnon mode	30 mW
T	Mechanical bath temperature	10 mK

FIG. 1. Robust entanglement of the CMM system. (a) Schematic diagram of the CMM system with double-pump lasers scheme. A highly polished YIG sphere is placed inside a three-dimensional microwave cavity, near the maximum magnetic field of the cavity, and simultaneously in a uniform static bias magnetic field of strength B_0 along the z axis, establishing the magnon-photon coupling. (b) Cartoon diagram of the interaction among the cavity, magnon, and mechanical modes. The magnon mode is directly driven by a microwave field to enhance the magnomechanical coupling, while the cavity mode is also driven simultaneously. (c) Frequency spectrum of this CMM system shown in panel (a). (d) The parameters selected for our numerical computations are practically achievable through experiments, and some of them are drawn from Refs. [61,83].

system [42–44], as well as photon blockade based on a periodically poled lithium niobate microcavity [45] or a linear cavity coupled to a nonlinear cavity [46]. Drawing inspiration from those earlier studies, we now demonstrate that the proposed approach can be effectively utilized to protect and potentially further enhance the robust magnon-photon, magnon-phonon, and photon-phonon entanglement, as well as the tripartite entanglement in a hybrid quantum CMM system. We observe that, by suitably adjusting the phase difference of the double-pump lasers, the three varied types of bipartite quantum entanglement and the tripartite quantum entanglement that exist within such a hybrid quantum CMM system can not only be effectively protected but also be significantly enhanced, while concurrently enhancing the system's robustness against thermal noises emanating from the environment. Our discoveries not only fall entirely within the scope of current experimental capabilities and demonstrate strong compatibility with other established methods for safeguarding quantum entanglement [47–60], but they also illuminate the path toward constructing an array of phase-controlled quantum CMM systems. The entanglement enhancement effect that is demonstrated lays a more favorable foundation for further applying this system to specific quantum technology tasks.

The structure of this paper unfolds as below. Section II presents the theoretical model of our hybrid CMM system and delves into a comprehensive analysis of its quantum dynamics. In Sec. III, we investigate the robust entanglement of magnon-photon, magnon-phonon, and photon-phonon under the influence of phase control. Ultimately, Sec. IV offers a concise summary of the entire article.

II. PHASE-CONTROLLED CMM SYSTEM: QUANTUM DYNAMICS

This study explores how to achieve coherent control and enhance the magnon-photon, magnon-phonon, and photon-phonon robust entanglement in such a hybrid quantum CMM system by modulating the relative phase in double-pump lasers. In particular, as depicted in Fig. 1(a), our research focuses on a hybrid CMM system where a polished YIG sphere is positioned within a three-dimensional microwave cavity [61]. A highly polished YIG sphere is essential to suppress two-magnon scattering and clamping losses [8,62], achieving narrow magnon linewidth and high mechanical quality factor [61], which are prerequisites for observing strong coupling and coherent magnomechanical effects. The Kittel mode of the YIG sphere (also known as the magnon mode) can be activated by a microwave drive field [63]. Additionally, the YIG sphere is subjected to a uniform static magnetic field (B_0) that serves to saturate its magnetization and create coupling between magnetic and microwave resonances [64]. As depicted in Fig. 1(b), the magnon mode and microwave cavity mode are coupled through magnetic dipole interaction. The magnon frequency ω_m is primarily governed by the gyromagnetic ratio ($\gamma/2\pi = 28$ GHz/T) and the external bias magnetic field [65], i.e., $\omega_m = \gamma B_0$. The YIG sphere exhibits magnetostriction [66–68], in which magnon excitation alters the magnetization, leading to corresponding geometric changes in the shape of the sphere. Concurrently, the mechanical deformation of the YIG sphere induced by an external magnetic field modulates its magnetization, giving rise to coupling between magnon and phonon modes [61,69,70]. The YIG sphere thus serves as a platform where magnon and phonon modes are simultaneously supported [61] and coupled through a nonlinear magnetostrictive interaction [see Fig. 1(b)]. In our system, the microwave photon wavelength is much larger than the YIG sphere size. Consequently, the radiation-pressure-induced direct coupling between photon and phonon is orders of magnitude weaker than the magnon-photon coupling and the magnon-phonon coupling, and can be safely neglected. All interactions depicted in Fig. 1(b) have been experimentally confirmed [8,70–72]. Within a rotating reference frame with the driving frequency ω_d, the effective Hamiltonian governing this CMM system can be written as

$$\begin{aligned} \hat{H} &= \hat{H}_0 + \hat{H}_{\text{int}} + \hat{H}_{\text{dr}}, \\ \hat{H}_0 &= \hbar\Delta_a\hat{a}^\dagger\hat{a} + \hbar\Delta_m\hat{m}^\dagger\hat{m} + \hbar\frac{\omega_b}{2}(\hat{q}^2 + \hat{p}^2), \\ \hat{H}_{\text{int}} &= \hbar g_{mb}\hat{m}^\dagger\hat{m}\hat{q} + \hbar g_{ma}(\hat{a}^\dagger\hat{m} + \hat{a}\hat{m}^\dagger), \\ \hat{H}_{\text{dr}} &= i\hbar(\varepsilon_a\hat{a}^\dagger e^{-i\theta_a} + \Omega_m\hat{m}^\dagger e^{-i\theta_m} - \text{H.c.}), \end{aligned} \tag{1}$$

where $\hat{a}$ ($\hat{a}^\dagger$) and $\hat{m}$ ($\hat{m}^\dagger$) denote the annihilation (creation) operators corresponding to the cavity mode (frequency ω_a) and magnon mode (frequency ω_m), respectively. $\Delta_a = \omega_a - \omega_d$ represents the optical detuning of the cavity mode relative to the driving cavity field. $\Delta_m = \omega_m - \omega_d$ characterizes the magnon-drive detuning between the magnon mode and the driving magnetic field. In the mechanical mode operating at resonance frequency ω_b, $\hat{q}$ and $\hat{p}$ denote the dimensionless position and momentum quadratures. Regarding the coupling parameters, g_{ma} and g_{mb} specify the magnon-microwave coupling rate and the single-magnon magnomechanical coupling rate, respectively. The phase and amplitude of the driving cavity field are characterized by θ_a and $|\varepsilon_a| = \sqrt{2\kappa_a P_a/\hbar\omega_d}$, where P_a represents the input laser power for the cavity mode and κ_a denotes the dissipation rate of the cavity mode. The phase and amplitude associated with the magnetic driving field are described by θ_m and $\Omega_m = \frac{\sqrt{5N}}{4}\gamma B_0$, with B_0 representing the external magnetic field, i.e., $B_0 = (1/R)\sqrt{(2p_m\mu_0/\pi c)}$, where R is the YIG sphere radius, μ_0 denotes vacuum permeability, c is the speed of electromagnetic waves in vacuum, and p_m represents the input laser power for the magnon mode. The total number of spins is given by $N = \rho V_m$, where V_m represents the volume of the YIG sphere and $\rho = 4.22 \times 10^{27}$ m^{-3} denotes its spin density [28]. The phase difference between the double-pump lasers is expressed as $\Delta\theta$, defined by the equation $\Delta\theta \equiv \theta_a - \theta_m$. By adjusting the phase difference $\Delta\theta$, the three varied types of bipartite quantum entanglement can be controlled.

Accounting for the impact of dissipations in the CMM system and environmental input noises, the dynamic evolution of the system is fully captured by the quantum Langevin equations (QLEs) expressed as

$$\begin{aligned} \dot{\hat{a}} &= -(i\Delta_a + \kappa_a)\hat{a} - ig_{ma}\hat{m} + \varepsilon_a e^{-i\theta_a} + \sqrt{2\kappa_a}\hat{a}^{\text{in}}, \\ \dot{\hat{m}} &= -(i\Delta_m + \kappa_m)\hat{m} - ig_{ma}\hat{a} - ig_{mb}\hat{m}\hat{q} + \Omega_m e^{-i\theta_m} \\ &\quad + \sqrt{2\kappa_m}\hat{m}^{\text{in}}, \\ \dot{\hat{q}} &= \omega_b\hat{p}, \\ \dot{\hat{p}} &= -\hat{q}\omega_b - g_{mb}\hat{m}^\dagger\hat{m} - \gamma_b\hat{p} + \hat{\xi}, \end{aligned} \tag{2}$$

where γ_b corresponds to the mechanical damping rate, κ_m signifies the dissipation rate of the magnon mode, and $\hat{a}^{\text{in}}$, $\hat{m}^{\text{in}}$, and $\hat{\xi}$ represent the vacuum noise operators associated with the cavity, magnon, and mechanical modes, respectively. The input vacuum noise operators exhibit zero-mean values, with their characteristics defined by the subsequent correlation functions [73]:

$$\begin{aligned} \langle\hat{a}^{\text{in}}(t)\hat{a}^{\text{in}\dagger}(t')\rangle &= [N_a(\omega_a) + 1]\delta(t - t'), \\ \langle\hat{a}^{\text{in}\dagger}(t)\hat{a}^{\text{in}}(t')\rangle &= N_a(\omega_a)\delta(t - t'), \\ \langle\hat{m}^{\text{in}}(t)\hat{m}^{\text{in}\dagger}(t')\rangle &= [N_m(\omega_m) + 1]\delta(t - t'), \\ \langle\hat{m}^{\text{in}\dagger}(t)\hat{m}^{\text{in}}(t')\rangle &= N_m(\omega_m)\delta(t - t'), \\ \langle\xi(t)\xi(t') + \xi(t')\xi(t)\rangle/2 &\simeq \gamma_b[2N_b(\omega_b) + 1]\delta(t - t'), \end{aligned} \tag{3}$$

where $N_j(\omega_{m_j}) = [\exp(\hbar\omega_{m_j}/k_B T) - 1]^{-1} (j = a, m, b)$ denotes the thermal mean occupation number for the photon, magnon, and phonon modes, respectively, with k_B representing the Boltzmann constant and T corresponding to the bath temperature. The approximation symbol "$\simeq$" in the last expression of Eq. (3) is employed since the mechanical noise correlation function is not strictly delta correlated, which indicates its non-Markovian nature [74,75]; it can be approximated as delta correlated only under the high mechanical quality factor approximation ($Q = \omega_m/\gamma_m \gg 1$), which is the Markovian approximation [76]. In contrast, the optical and magnon noise correlations are exact delta functions. In the regime of strong driving fields, each operator in the CMM system can be decomposed into its steady-state mean value plus a small quantum fluctuation term, i.e.,

$$\begin{aligned} \hat{a} &= \alpha_s + \delta\hat{a}, \quad \hat{m} = m_s + \delta\hat{m}, \\ \hat{q} &= q_s + \delta\hat{q}, \quad \hat{p} = p_s + \delta\hat{p}. \end{aligned} \tag{4}$$

Upon substituting Eq. (4) into QLEs (2), we derive the first-order inhomogeneous differential equations that the steady-state mean values, i.e.,

$$\begin{aligned} \dot{\alpha}_s &= -(i\Delta_a + \kappa_a)\alpha_s - ig_{ma}m_s + \varepsilon_a e^{-i\theta_a}, \\ \dot{m}_s &= -(i\Delta_m + \kappa_m)m_s - ig_{ma}\alpha_s - ig_{mb}m_s q_s + \Omega_m e^{-i\theta_m}, \\ \dot{q}_s &= \omega_b p_s, \\ \dot{p}_s &= -q_s\omega_b - g_{mb}|m_s|^2. \end{aligned} \tag{5}$$

The linearized QLEs that quantum fluctuations can be expressed as

$$\begin{aligned}\delta\dot{\hat{a}} &= -(i\Delta_a+\kappa_a)\delta\hat{a} - ig_{ma}\delta\hat{m} + \sqrt{2\kappa_a}\hat{a}^{\text{in}},\\ \delta\dot{\hat{m}} &= -(i\Delta_m+\kappa_m)\delta\hat{m} - ig_{ma}\delta\hat{a} - ig_{mb}m_s\delta\hat{q}\\ &\quad - ig_{mb}\delta\hat{m}q_s + \sqrt{2\kappa_m}\hat{m}^{\text{in}},\\ \delta\dot{\hat{q}} &= \omega_b\delta\hat{p},\\ \delta\dot{\hat{p}} &= -\omega_b\delta\hat{q} - g_{mb}m_s^\dagger\delta\hat{m} - g_{mb}m_s\delta\hat{m}^\dagger - \gamma_b\delta\hat{p} + \hat{\xi}.\end{aligned} \tag{6}$$

Setting the derivatives of Eq. (5) to zero allows calculation of the mean values for each mode at steady state:

$$\begin{aligned}\alpha_s &= -\frac{ig_{ma}m_s - \varepsilon_a e^{-i\theta_a}}{i\Delta_a+\kappa_a},\\ q_s &= -\frac{g_{mb}|m_s|^2}{\omega_b},\\ m_s &= \frac{-ig_{ma}\varepsilon_a e^{-i\theta_a} + (i\Delta_a+\kappa_a)\Omega_m e^{-i\theta_m}}{(i\tilde{\Delta}_m+\kappa_m)(i\Delta_a+\kappa_a)+g_{ma}^2},\end{aligned} \tag{7}$$

where $\tilde{\Delta}_m = \Delta_m + g_{mb}q_s$ represents the effective magnon-drive detuning. Additionally, since $|\tilde{\Delta}_m|, |\Delta_a| \gg \kappa_a, \kappa_m$, the steady-state mean values for the magnon mode may be expressed in the following simplified form:

$$m_s = \frac{i\Delta_a\Omega_m e^{-i\theta_m} - ig_{ma}\varepsilon_a e^{-i\theta_a}}{g_{ma}^2 - \tilde{\Delta}_m\Delta_a}. \tag{8}$$

It can be seen that m_s is jointly determined by θ_m and θ_a. From the aforementioned linearized QLEs, i.e., Eq. (6), one can derive the corresponding linearized system Hamiltonian:

$$\begin{aligned}\hat{H}^{\text{lin}} &= \hat{H}_0^{\text{lin}} + \hat{H}_{ma}^{\text{lin}} + \hat{H}_{mb}^{\text{lin}},\\ \hat{H}_0^{\text{lin}} &= \hbar\Delta_a\delta\hat{a}^\dagger\delta\hat{a} + \hbar\Delta_m\delta\hat{m}^\dagger\delta\hat{m} + \hbar\frac{\omega_b}{2}(\delta\hat{q}^2+\delta\hat{p}^2),\\ \hat{H}_{ma}^{\text{lin}} &= \hbar g_{ma}(\delta\hat{a}^\dagger\delta\hat{m} + \delta\hat{m}^\dagger\delta\hat{a}),\\ \hat{H}_{mb}^{\text{lin}} &= \hbar g_{mb}(m_s^*\delta\hat{m}\delta\hat{q} + m_s\delta\hat{m}^\dagger\delta\hat{q} + q_s\delta\hat{m}^\dagger\delta\hat{m}).\end{aligned} \tag{9}$$

It is noteworthy that the magnon and mechanical modes coupling term in Eq. (9) appears in the form of $\hat{H}_{mb}^{\text{lin}} = \hbar g_{mb}(m_s^*\delta\hat{m}\delta\hat{q} + m_s\delta\hat{m}^\dagger\delta\hat{q} + q_s\delta\hat{m}^\dagger\delta\hat{m})$. The position operator of the mechanical oscillator $\delta\hat{q} = (\delta\hat{b}+\delta\hat{b}^\dagger)/\sqrt{2}$ simultaneously contains both the annihilation operator $\hat{b}$ and the creation operator $\hat{b}^\dagger$ for the phonon mode. Substitute it into the magnon and mechanical modes coupling term in Eq. (9), and we obtain

$$\begin{aligned}\hat{H}_{mb}^{\text{lin}} &= \frac{\hbar g_{mb}}{\sqrt{2}}(m_s^*\delta\hat{m}\delta\hat{b} + m_s\delta\hat{m}^\dagger\delta\hat{b}^\dagger)\\ &\quad + \frac{\hbar g_{mb}}{\sqrt{2}}(m_s^*\delta\hat{m}\delta\hat{b}^\dagger + m_s\delta\hat{m}^\dagger\delta\hat{b})\\ &\quad + \hbar g_{mb}q_s\delta\hat{m}^\dagger\delta\hat{m},\end{aligned} \tag{10}$$

the magnon and mechanical modes are coupled via two kinds of interactions: (1) a parametric down-conversion-type process characterized by $m_s^*\delta\hat{m}\delta\hat{b} + m_s\delta\hat{m}^\dagger\delta\hat{b}^\dagger$ and (2) a beam-splitter-type process characterized by $m_s^*\delta\hat{m}\delta\hat{b}^\dagger + m_s\delta\hat{m}^\dagger\delta\hat{b}$. The parametric down-conversion is precisely the source of entanglement generation between the magnon and mechanical modes, while the beam splitter will transfer this entanglement to the cavity mode. Importantly, the steady-state mean value of the magnon mode m_s depends on the phase difference (i.e., $\Delta\theta \equiv \theta_a - \theta_m$) [see Eq. (8)]. As can be seen from Eq. (10), the intensity of the parametric down-conversion is proportional to $|m_s|$. Therefore, the phase difference $\Delta\theta$ of driving fields first influences the steady-state mean value of the magnon mode. Subsequently, the phase difference $\Delta\theta$ influences the weight of the parametric down-conversion in the total interaction. Finally, the phase difference $\Delta\theta$ influences the logarithmic negativity E_N, i.e., Eq. (25).

Introducing the operators for optical and magnon quadrature fluctuations, defined as

$$\begin{aligned}\delta\hat{X} &= \frac{\delta\hat{a}+\delta\hat{a}^\dagger}{\sqrt{2}}, \quad \delta\hat{Y} = \frac{\delta\hat{a}-\delta\hat{a}^\dagger}{i\sqrt{2}},\\ \delta\hat{x} &= \frac{\delta\hat{m}+\delta\hat{m}^\dagger}{\sqrt{2}}, \quad \delta\hat{y} = \frac{\delta\hat{m}-\delta\hat{m}^\dagger}{i\sqrt{2}},\end{aligned} \tag{11}$$

along with the corresponding input noise operators, formulated as

$$\begin{aligned}\delta\hat{X}^{\text{in}} &= \frac{\delta\hat{a}^{\text{in}}+\delta\hat{a}^{\text{in},\dagger}}{\sqrt{2}}, \quad \delta\hat{Y}^{\text{in}} = \frac{\delta\hat{a}^{\text{in}}-\delta\hat{a}^{\text{in},\dagger}}{i\sqrt{2}},\\ \delta\hat{x}^{\text{in}} &= \frac{\delta\hat{m}^{\text{in}}+\delta\hat{m}^{\text{in},\dagger}}{\sqrt{2}}, \quad \delta\hat{y}^{\text{in}} = \frac{\delta\hat{m}^{\text{in}}-\delta\hat{m}^{\text{in},\dagger}}{i\sqrt{2}},\end{aligned} \tag{12}$$

the associated linearized QLEs can be written explicitly in a concise form as

$$\dot{\hat{u}}(t) = A\hat{u}(t) + \hat{v}(t), \tag{13}$$

where we introduce the fluctuation operator vector $\hat{u}$,

$$\hat{u}^T(t) = (\delta\hat{X}, \delta\hat{Y}, \delta\hat{x}, \delta\hat{y}, \delta\hat{q}, \delta\hat{p}), \tag{14}$$

and the input noise operator $\hat{v}$,

$$\hat{v}^T(t) = (\sqrt{2\kappa_a}\hat{X}^{\text{in}}, \sqrt{2\kappa_a}\hat{Y}^{\text{in}}, \sqrt{2\kappa_m}\hat{x}^{\text{in}}, \sqrt{2\kappa_m}\hat{y}^{\text{in}}, 0, \hat{\xi}). \tag{15}$$

The corresponding coefficient matrix A is given by

$$A = \begin{pmatrix} -\kappa_a & \Delta_a & 0 & g_{ma} & 0 & 0\\ -\Delta_a & -\kappa_a & -g_{ma} & 0 & 0 & 0\\ 0 & g_{ma} & -\kappa_m & \tilde{\Delta}_m & -G_{mb} & 0\\ -g_{ma} & 0 & -\tilde{\Delta}_m & -\kappa_m & 0 & 0\\ 0 & 0 & 0 & 0 & 0 & \omega_m\\ 0 & 0 & 0 & G_{mb} & -\omega_b & -\gamma_b \end{pmatrix}, \tag{16}$$

and $G_{mb} = i\sqrt{2}g_{mb}m_s$ denotes the effective magnomechanical coupling rate. The effective magnomechanical coupling rate can be adjusted by the phase difference $\Delta\theta$, which forms the basis for the manipulation of the magnon-photon, magnon-phonon, and photon-phonon robust entanglement. The phase difference $\Delta\theta$ of driving fields first influences the steady-state mean values of the magnon mode [i.e., Eq. (8)]. Thereafter, the phase difference modulates both the effective magnomechanical coupling rate ($G_{mb} = i\sqrt{2}g_{mb}m_s$) and the corresponding coefficient matrix, which is specifically shown in Eq. (16). Eventually, the phase difference modulates the logarithmic negativity [i.e., Eq. (25)]. Furthermore, the solution to the linearized QLEs (13) can be obtained as

$$\hat{u}(t) = \mathcal{M}(t)\hat{u}(0) + \int_0^t d\tau \mathcal{M}(\tau)\hat{v}(t-\tau), \tag{17}$$

where

$$\mathcal{M}(t) = \exp(At). \tag{18}$$

The system is stable only when all real parts of the eigenvalues of A are negative, as determined by the Routh-Hurwitz criterion [77]. Upon fulfillment of all the stability conditions, we can obtain $\mathcal{M}(\infty) = 0$ in the steady state, and

$$\hat{u}_i(\infty) = \int_0^\infty d\tau \sum_k \mathcal{M}_{ik}(\tau)\hat{v}_k(t-\tau). \tag{19}$$

Due to the linearized dynamics and the Gaussian nature of the quantum noise, the steady state of the quantum fluctuations within the CMM system can finally evolve into a quadripartite zero-mean Gaussian state, which is fully characterized by a 6×6 correlation matrix (CM) V with its components defined as

$$V_{kl} = \langle \hat{u}_k(\infty)\hat{u}_l(\infty) + \hat{u}_l(\infty)\hat{u}_k(\infty)\rangle/2. \tag{20}$$

By substituting Eq. (19) into Eq. (20) and using the fact that the six components of $\hat{v}(t)$ are not correlated with each other, the steady-state CM V is given by

$$V = \int_0^\infty d\tau \mathcal{M}(\tau) D \mathcal{M}^{\mathrm{T}}(\tau), \tag{21}$$

where

$$\begin{aligned} D = \mathrm{Diag}\,[&\kappa_a(2N_a+1), \kappa_a(2N_a+1), \kappa_m(2N_m+1),\\ &\kappa_m(2N_m+1), 0, \gamma_b(2N_b+1)] \end{aligned} \tag{22}$$

is a diffusion matrix that is obtained by using

$$\langle \hat{v}_k(\tau)\hat{v}_l(\tau') + \hat{v}_l(\tau')\hat{v}_k(\tau)\rangle/2 = D_{kl}\delta(\tau-\tau'). \tag{23}$$

Given the stability condition, the steady-state covariance matrix CM V satisfies the Lyapunov equation [76]:

$$AV + VA^{\mathrm{T}} = -D. \tag{24}$$

The Lyapunov equation (24) is a linear equation and allows us to derive CM V for any relevant parameters. However, the analytical expression of V is too complicated and thus would not be reported here.

III. RESULTS AND DISCUSSIONS

For quantifying bipartite entanglement in a three-mode continuous variable system, we can adopt the logarithmic negativity E_N as an effective measure, which can be defined as [78]

$$E_N = \max\,[0, -\ln(2\nu^-)], \tag{25}$$

where

$$\nu^- = 2^{-1/2}\{\Sigma(V') - [\Sigma(V')^2 - 4\det V']^{1/2}\}^{1/2}, \tag{26}$$

with

$$\Sigma(V') = \det\mathcal{A} + \det\mathcal{B} - 2\det\mathcal{C}. \tag{27}$$

Here, ν^- is the smallest symplectic eigenvalue of the partial transpose of a reduced 4×4 CM V'. The reduced CM V' contains the entries of V, and it can be directly derived by selecting the rows and columns of the interesting mode. By writing the reduced CM V' in a 2×2 block form, we have

$$V' = \begin{pmatrix} \mathcal{A} & \mathcal{C} \\ \mathcal{C}^{\mathrm{T}} & \mathcal{B} \end{pmatrix}. \tag{28}$$

Equation (23) indicates that the CMM entanglement emerge only when $\nu^- < 1/2$, which is equivalent to Simon's necessary and sufficient entanglement nonpositive partial transpose criterion (or the related Peres-Horodecki criterion) for certifying bipartite entanglement in Gaussian states [79].

In order to investigate the tripartite quantum entanglement in the three-mode CMM system, we employ a quantitative measure, specifically the minimum residual contangle $\mathcal{R}_\tau^{\min}$ [80,81]. This measure is defined as follows:

$$\mathcal{R}_\tau^{\min} \equiv \min_{(r,s,t)} \left[E_\tau^{r|st} - E_\tau^{r|s} - E_\tau^{r|t}\right], \tag{29}$$

in this context, $(r,s,t) \in \{a,m,b\}$ denotes all the possible permutations of the three-mode indices. Meanwhile, $E_\tau^{u|v}$ is the contangle of subsystems of u (with one mode) and v (with one or two modes), which can be characterized by an appropriate entanglement monotone, such as the squared logarithmic negativity.

$$E_\tau^{u|v} \equiv [E_N]^2 \equiv \{\max\,[0, -\ln(2\tilde{\nu}_-)]\}^2. \tag{30}$$

Here, $\tilde{\nu}_-$ stands for the minimum symplectic eigenvalue associated with the CM. In the case where v encompasses only a single mode, the expression for $\tilde{\nu}_-$ in Eq. (30) is given by

$$\tilde{\nu}_- = \min\,[\mathrm{eig}|i\Omega_2\tilde{V}_4|], \tag{31}$$

where

$$\Omega_2 = \oplus_{j=1}^2 i\sigma_y, \tag{32}$$

where σ_y represents the Pauli y matrix. The matrix $\tilde{V}_4$ shown in Eq. (31) can be written as

$$\tilde{V}_4 = P_0 V_4 P_0, \tag{33}$$

here, V_4 represents the 4×4 CM of two subsystems. This matrix is obtained by removing the rows and columns that correspond to the uninteresting mode from the matrix V, and

$$P_0 = \mathrm{diag}(1, -1, 1, 1), \tag{34}$$

refers to the matrix that accomplishes the partial transposition operation when applied to CMs.

When v contains two modes, $\tilde{\nu}_-$ in Eq. (30) is obtained by

$$\tilde{\nu}_- = \min\,[\mathrm{eig}|i\Omega_3\tilde{V}_6|], \tag{35}$$

where

$$\Omega_3 = \oplus_{j=1}^3 i\sigma_y, \tag{36}$$

and the matrix $\tilde{V}_6$ in Eq. (35) is obtained by

$$\tilde{V}_6 = P_{r|(st)} V_6 P_{r|(st)}, \tag{37}$$

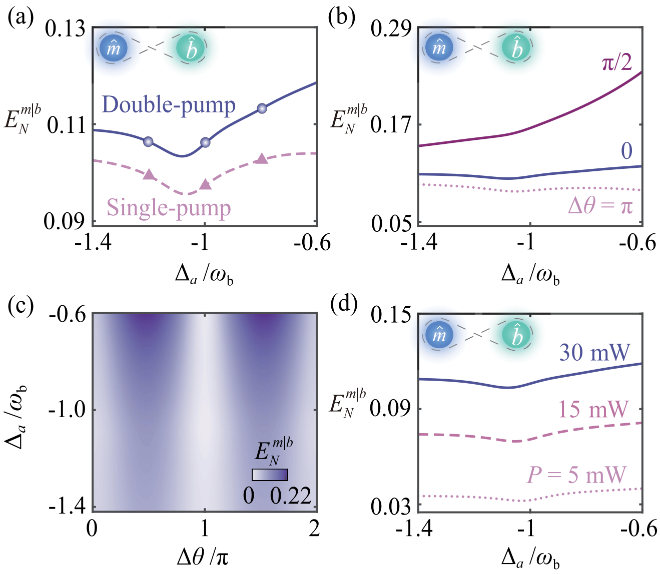

FIG. 2. Phase-controlled robust entanglement between magnon and mechanical modes through adjusting the phase difference $\Delta\theta$ of driving fields. (a) The logarithmic negativity $E_N^{m|b}$ vs the optical detuning Δ_a/ω_b for the single-pump case ($P_m = 30$ mW and $P_a = 0$) and the double-pump case ($P_m = 30$ mW and $P_a = 30$ mW). (b) $E_N^{m|b}$ vs Δ_a/ω_b for different $\Delta\theta$. (c) Density plot of $E_N^{m|b}$ as a function of $\Delta\theta$ and Δ_a/ω_b. (d) $E_N^{m|b}$ vs Δ_a/ω_b for different input laser power ($P = P_m = P_a$), with $\Delta\theta = 0$. We select $\tilde{\Delta}_m/\omega_b = 0.9$. The other parameters are provided in the text.

where V_6 represents the 6×6 CM of this system and we introduce the partial transposition matrices

$$\begin{aligned} P_{a|mb} &= \mathrm{diag}(1, -1, 1, 1, 1, 1), \\ P_{m|ab} &= \mathrm{diag}(1, 1, 1, -1, 1, 1), \\ P_{b|am} &= \mathrm{diag}(1, 1, 1, 1, 1, -1). \end{aligned} \tag{38}$$

The residual contangle adheres to the principle of monogamy in quantum entanglement, i.e.,

$$E_\tau^{r|st} - E_\tau^{r|s} - E_\tau^{r|t} \geqslant 0. \tag{39}$$

This inequality bears a resemblance to the Coffman-Kundu-Wootters monogamy inequality [82], which holds for three qubits. The fact that the nonzero minimum residual contangle $\mathcal{R}_\tau^{\min} > 0$ indicates the emergence of complete tripartite inseparability.

Now, we thoroughly explore the magnon-photon, magnon-phonon, and photon-phonon robust entanglement of this hybrid CMM system in detail. In our numerical computations, we utilize the following parameters to guarantee the stability and practical viability of this CMM system [61,83]. The parameters are $\omega_a/2\pi = 10$ GHz, $\omega_b/2\pi = 10$ MHz, $\omega_m/2\pi = 10.1$ GHz, $\kappa_m/2\pi = 1$ MHz, $\kappa_a/2\pi = 1$ MHz, $\gamma_b/2\pi = 100$ Hz, $g_{mb}/2\pi = 0.3$ MHz, $g_{ma}/2\pi = 1$ MHz, $R = 250$ μm, $P_m = 30$ mW, $P_a = 30$ mW, and $T = 10$ mK.

In Fig. 2, we first explore how to regulate the behavior of the bipartite entanglement between the magnon and mechanical modes by tuning the phase difference $\Delta\theta$ of the two driving lasers. Specifically, the logarithmic negativity $E_N^{m|b}$ is represented as a function of the optical detuning Δ_a/ω_b under the single-pump laser case ($P_m = 30$ mW and $P_a = 0$) [see the dashed curves in Fig. 2(a)]. Additionally, we plot the logarithmic negativity $E_N^{m|b}$ as a function of the optical detuning Δ_a/ω_b under the double-pump laser case ($P_m = 30$ mW and $P_a = 30$ mW) [see the solid curves in Fig. 2(a)]. It is demonstrated that at a specific phase difference $\Delta\theta$ of the two driving lasers, such as $\Delta\theta = 0$, the double-pump laser case can generate more robust bipartite entanglement between the magnon and mechanical modes compared to the single-pump laser case. In Fig. 2(b), we plot the logarithmic negativity $E_N^{m|b}$ as a function of the optical detuning Δ_a/ω_b for various values of the phase difference $\Delta\theta$ of the two driving lasers. As observed, the logarithmic negativity $E_N^{m|b}$ can be effectively modulated or even enhanced by adjusting the phase difference $\Delta\theta$. In particular, the entanglement degree between the magnon and mechanical modes is enhanced when $\Delta\theta = \pi/2$ compared to when $\Delta\theta = \pi$. Interference occurs between two pump lasers with the same frequency, which manifests as either constructive or destructive interference. The bipartite entanglement between magnon and mechanical modes can be enhanced or suppressed through constructive or destructive interference pathways. The relative phase plays a critical role in controlling interference. By intentionally designing the relative phase, we can effectively control the bipartite entanglement. When $\Delta\theta = \pi/2$, the constructive interference reaches its maximum, leading to the strongest entanglement. In order to clearly observe how the phase difference $\Delta\theta$ regulates the bipartite entanglement between the magnon and mechanical modes, we present the dependence of the logarithmic negativity $E_N^{m|b}$ on both $\Delta\theta$ and the optical detuning Δ_a/ω_b in Fig. 2(c). It can be seen from the figure that by tuning the phase difference $\Delta\theta$ of the driving lasers, $E_N^{m|b}$ can be effectively regulated. Figure 2(d) shows the influence of the driving power of the double-pump system on the magnon-phonon entanglement, with $\Delta\theta = 0$. From the obtained results, it is evident that an increase in the driving power brings about a concurrent elevation in the maximum value of the magnon-phonon entanglement.

In Fig. 3, we investigate how to regulate the bipartite entanglement between the magnon and cavity modes by adjusting the phase difference $\Delta\theta$ of the two driving lasers. As shown in Fig. 3(a), we plot the logarithmic negativity $E_N^{m|a}$ as a function of the optical detuning Δ_a/ω_b for both the double-pump ($P_m = 30$ mW and $P_a = 30$ mW) and single-pump laser cases ($P_m = 30$ mW and $P_a = 0$ mW). When the phase difference $\Delta\theta$ of the two driving lasers is tuned to a special value $\Delta\theta = 0$, the double-pump laser case induces stronger magnon-photon entanglement than the single-pump case [see Fig. 3(a)]. In Fig. 3(b), we plot the logarithmic negativity $E_N^{m|a}$ as a function of the optical detuning Δ_a/ω_b for different values of the phase difference $\Delta\theta$. It can be observed that the maximum entanglement degree between the magnon and cavity modes occurs near $\Delta_a/\omega_b \simeq -1$. Moreover, $E_N^{m|a}$ can be effectively modulated or enhanced by adjusting $\Delta\theta$. We find that the entanglement reaches its maximum value at an optimal $\Delta\theta = 0$, which is enhanced compared to the cases of $\Delta\theta = \pi/2$ or π. To gain a clearer understanding of how $\Delta\theta$ modulates the entanglement, we additionally show the

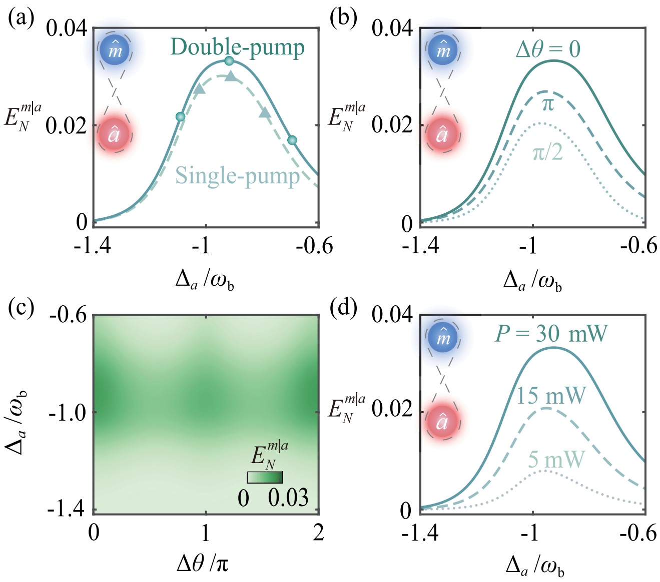

FIG. 3. Phase-controlled robust entanglement between magnon and cavity modes by adjusting the phase difference $\Delta\theta$ of driving fields. (a) The logarithmic negativity $E_N^{m|a}$ vs the optical detuning Δ_a/ω_b for with the single-pump case ($P_m = 30\,\mathrm{mW}$ and $P_a = 0$) and the double-pump case ($P_m = 30\,\mathrm{mW}$ and $P_a = 30\,\mathrm{mW}$). (b) $E_N^{m|a}$ vs Δ_a/ω_b for different $\Delta\theta$. (c) Density plot of $E_N^{m|a}$ as a function of $\Delta\theta$ and Δ_a/ω_b. (d) $E_N^{m|a}$ vs Δ_a/ω_b for different input laser power ($P = P_m = P_a$), with $\Delta\theta = 0$. The other parameters are provided in the text.

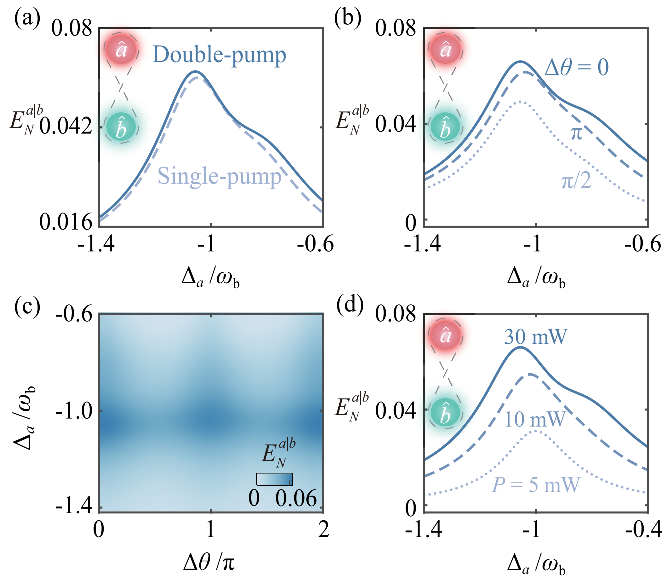

FIG. 4. Phase-controlled robust entanglement between cavity and mechanical modes by tuning the phase difference $\Delta\theta$ of driving fields. (a) The logarithmic negativity $E_N^{a|b}$ vs the optical detuning Δ_a/ω_b for the single-pump case ($P_m = 30\,\mathrm{mW}$ and $P_a = 0$) and the double-pump case ($P_m = 30\,\mathrm{mW}$ and $P_a = 30\,\mathrm{mW}$). (b) $E_N^{a|b}$ vs Δ_a/ω_b for different $\Delta\theta$. (c) Density plot of $E_N^{a|b}$ as a function of $\Delta\theta$ and Δ_a/ω_b. (d) $E_N^{a|b}$ vs Δ_a/ω_b for different input laser power ($P = P_m = P_a$), with $\Delta\theta = 0$. The other parameters are provided in the text.

dependence of $E_N^{m|a}$ on Δ_a/ω_b and $\Delta\theta$ in Fig. 3(c). Figure 3(d) shows the influence of the driving power of the double-pump system on the magnon-photon entanglement, with $\Delta\theta = 0$. The results clearly show that an increase in the driving power leads to a concurrent elevation in the maximum value of the magnon-photon entanglement.

In Fig. 4, we study how to regulate the photon-phonon entanglement via tuning the phase difference $\Delta\theta$ of the two driving lasers. Specifically, as depicted in Fig. 4(a), the logarithmic negativity $E_N^{a|b}$ is presented as a function of the optical detuning Δ_a/ω_b in the double-pump laser case ($P_m = 30\,\mathrm{mW}$ and $P_a = 30\,\mathrm{mW}$). In the single-pump laser scenario ($P_m = 30\,\mathrm{mW}$ and $P_a = 0$), we also plot the logarithmic negativity $E_N^{a|b}$ versus the optical detuning Δ_a/ω_b. As illustrated in Fig. 4(a), for a specific phase difference, e.g., $\Delta\theta = 0$, the double-pump laser case can generate more robust entanglement than the single-pump case. As demonstrated in Fig. 4(b), we plot the logarithmic negativity $E_N^{a|b}$ as a function of the optical detuning Δ_a/ω_b for a range of phase differences $\Delta\theta$. It is shown that the degree of such cavity photon-phonon entanglement is the greatest near the optical detuning $\Delta_a/\omega_b \simeq -1$. When adjusting the phase difference $\Delta\theta$, $E_N^{a|b}$ can be effectively modulated or even enhanced at specific values of phase difference $\Delta\theta$. We find that the photon-phonon entanglement could be enhanced at $\Delta\theta = 0$ compared to $\Delta\theta = \pi/2$ or π [see Fig. 4(b)]. To observe this effect more clearly, we additionally show the dependence of the logarithmic negativity $E_N^{a|b}$ on the optical detuning Δ_a/ω_b and the phase difference $\Delta\theta$ in Fig. 4(c). As shown, the logarithmic negativity $E_N^{a|b}$ can be well regulated periodically by adjusting the phase difference $\Delta\theta$ between the two driving lasers. In Fig. 4(d), the logarithmic negativity $E_N^{a|b}$ is plotted as a function of the optical detuning Δ_a/ω_b for different values of the driving power with the phase difference $\Delta\theta = 0$. From the obtained results, it is clear that an increase in the driving power brings about a concurrent elevation in the maximum value of the entanglement.

In Fig. 5(a), the logarithmic negativity $E_N^{m|b}$, $E_N^{a|b}$, and $E_N^{m|a}$ are plotted as a function of the optical detuning Δ_a/ω_b with the phase difference values $\Delta\theta = 0$ in the double-pump laser case ($P_m = 30\,\mathrm{mW}$ and $P_a = 30\,\mathrm{mW}$). This indicates that in a parameter regime around $\Delta_a/\omega_b = -1$, all bipartite entanglements can be simultaneously present. The magnomechanical (radiation pressurelike) interaction leads to significant cooling of the mechanical mode and, at the same time, induces considerable magnomechanical entanglement owing to the strong coupling [28]. The complementary relation of the solid curve and the dashed and dotted curves in Fig. 5(a) indicates that the photon-phonon and magnon-photon entanglement are transferred from the magnon-phonon entanglement. In Fig. 5(b), the logarithmic negativity $E_N^{m|b}$, $E_N^{a|b}$, and $E_N^{m|a}$ are plotted as a function of the phase difference values $\Delta\theta$ with the optical detuning $\Delta_a/\omega_b = -1$. As can be seen from Fig. 5(b), within the phase difference range of $\Delta\theta$ from 0 to $\pi/2$, the magnon-phonon entanglement strength increases with increasing phase difference, while the photon-phonon entanglement and the magnon-photon entanglement decrease accordingly; whereas within the $\Delta\theta$ range from $\pi/2$ to π, the magnon-phonon entanglement

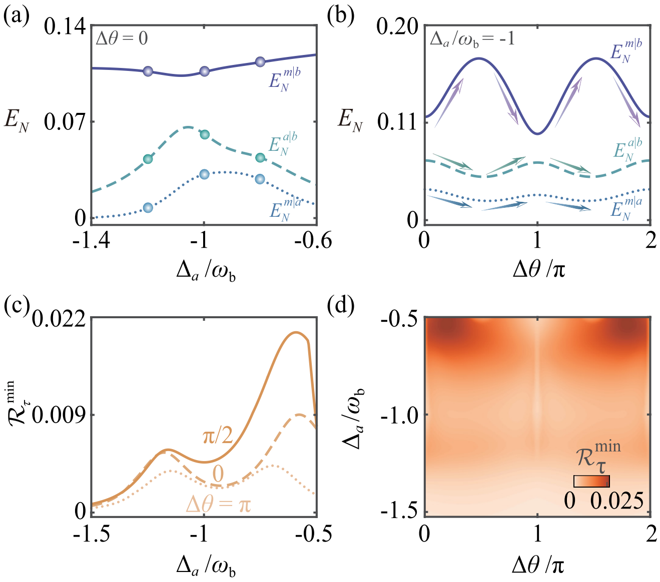

FIG. 5. (a) The logarithmic negativity $E_N^{m|b}$ (solid), $E_N^{a|b}$ (dashed), and $E_N^{m|a}$ (dotted) vs the optical detuning Δ_a/ω_b with the phase difference $\Delta\theta = 0$. (b) $E_N^{m|b}$, $E_N^{a|b}$, and $E_N^{m|a}$ vs $\Delta\theta$ with $\Delta_a/\omega_b = -1$. (c) The minimum residual contangle $\mathcal{R}_\tau^{\min}$ vs Δ_a/ω_b for different $\Delta\theta$. (d) Density plot of $\mathcal{R}_\tau^{\min}$ as a function of $\Delta\theta$ and Δ_a/ω_b. We select $g_{mb}/2\pi = 0.7$ MHz. The other parameters are provided in the text.

strength decreases with increasing phase difference, while the photon-phonon entanglement and magnon-photon entanglement increase accordingly. Apart from the manipulation of all bipartite entanglements, the phase difference can also manipulate the tripartite entanglement of the system. In Fig. 5(c), the minimum residual contangle $\mathcal{R}_\tau^{\min}$ is plotted as a function of the optical detuning Δ_a/ω_b for different phase difference values $\Delta\theta$ in the double-pump laser case ($P_m = 30$ mW and $P_a = 30$ mW). It can be seen that when adjusting the phase difference $\Delta\theta$ of the driving fields, the minimum residual contangle $\mathcal{R}_\tau^{\min}$ can be modulated well [see Fig. 5(c)]. In particular, the tripartite CMM entanglement could be considerably enhanced for the phase difference $\Delta\theta = \pi/2$ compared with that of the phase difference $\Delta\theta = \pi$. Moreover, it can be seen that the variation trend of the tripartite entanglement of the system with the optical detuning is consistent with that of the magnon-phonon entanglement. To see the regulation of the phase difference $\Delta\theta$ on the tripartite CMM entanglement more clearly, we show in Fig. 5(d) how the minimum residual contangle $\mathcal{R}_\tau^{\min}$ depends on the phase difference $\Delta\theta$ and the optical detuning Δ_a/ω_b. It can be seen that by adjusting the phase difference $\Delta\theta$ between the driving lasers, the minimum residual contangle $\mathcal{R}_\tau^{\min}$ can be effectively regulated.

IV. CONCLUSION

In conclusion, we have studied how to generate, manipulate, and even enhance the robust magnon-photon, magnon-phonon, and photon-phonon entanglement, as well as the tripartite entanglement. This was achieved by properly adjusting the phase difference $\Delta\theta$ of the dual-pump lasers within the hybrid cavity CMM system. Our findings reveal that all three types of bipartite entanglement and the tripartite entanglement can be bolstered, and their resilience to thermal noise can also be enhanced through fine-tuning the phase difference $\Delta\theta$ of the driving lasers. Our research results illuminate potential strategies for safeguarding and optimizing the functionality of diverse quantum devices amidst the challenges posed by real-world noisy conditions. These insights offer a promising pathway to the realization of a variety of quantum technologies that leverage entanglement, encompassing quantum computing [84–86], quantum sensing [87–90], and quantum networking [91–94]. From a more expansive perspective, we foresee the potential for our research to be further developed, enabling the exploration of a diverse array of other quantum phenomena utilizing these CMM systems. These may encompass the generation of ultraslow light [95–97], magnon blockade effects [98–100], and ultrahigh-sensitivity sensing [101–103].

ACKNOWLEDGMENTS

This work was supported by the National Natural Science Foundation of China (Grants No. 12565001, No. 12205054, No. 12074106, and No. 12347136), the Postdoctoral Fellowship Program (Grade C) of China Postdoctoral Science Foundation (Grant No. GZC20231726), the Natural Science Foundation of Henan Province (Grant No. 242300421165), the Henan Province Postdoctoral Research Funding Project (Grant No. HN2025011), and the Natural Science Foundation of Jiangxi Province (Grant No. 20252BAC200163).

DATA AVAILABILITY

The data that support the findings of this article are not publicly available. The data are available from the authors upon reasonable request.

[1] X. Zuo, Z.-Y. Fan, H. Qian, M.-S. Ding, H. Tan, H. Xiong, and J. Li, Cavity magnomechanics: From classical to quantum, New J. Phys. **26**, 031201 (2024).

[2] H.-Y. Yuan, Y.-S. Cao, A. Kamra, R. A. Duine, and P. Yan, Quantum magnonics: When magnon spintronics meets quantum information science, Phys. Rep. **965**, 1 (2022).

[3] S. P. Wolski, D. Lachance-Quirion, Y. Tabuchi, S. Kono, A. Noguchi, K. Usami, and Y. Nakamura, Dissipation-based quantum sensing of magnons with a superconducting qubit, Phys. Rev. Lett. **125**, 117701 (2020).

[4] L.-Q. Dany, T. Yutaka, G. Arnaud, U. Koji, and N. Yasunobu, Hybrid quantum systems based on magnonics, Appl. Phys. Express **12**, 070101 (2019).

[5] D. Lachance-Quirion, Y. Tabuchi, S. Ishino, A. Noguchi, T. Ishikawa, R. Yamazaki, and Y. Nakamura, Resolving quanta of collective spin excitationsin a millimeter-sized ferromagnet, Sci. Adv. **3**, e1603150 (2017).

[6] Y. Tabuchi, S. Ishino, T. Ishikawa, R. Yamazaki, K. Usami, and Y. Nakamura, Hybridizing ferromagnetic magnons and microwave photons in the quantum limit, Phys. Rev. Lett. **113**, 083603 (2014).
[7] B. Z. Rameshti, S. V. Kusminskiy, J. A. Haigh, K. Usami, D. Lachance-Quirion, Y. Nakamura, C.-M. Hu, H. X. Tang, G. E. W. Bauer, and Y. M. Blanter, Cavity magnonics, Phys. Rep. **979**, 1 (2022).
[8] C. A. Potts, E. Varga, V. A. S. V. Bittencourt, S. V. Kusminskiy, and J. P. Davis, Dynamical backaction magnomechanics, Phys. Rev. X **11**, 031053 (2021).
[9] X. Zhang, C.-L. Zou, L. Jiang, and H. X. Tang, Strongly coupled magnons and cavity microwave photons, Phys. Rev. Lett. **113**, 156401 (2014).
[10] A. Kani, B. Sarma, and J. Twamley, Intensive cavity-magnomechanical cooling of a levitated macromagnet, Phys. Rev. Lett. **128**, 013602 (2022).
[11] Y. Wang, H.-L. Zhang, J.-L. Wu, J. Song, K. Yang, W. Qin, H. Jing, and L.-M. Kuang, Quantum parametric amplification of phonon-mediated magnon-spin interaction, Sci. China Phys. Mech. Astron. **66**, 110311 (2023).
[12] J. Li, Y.-P. Wang, J.-Q. You, and S.-Y. Zhu, Squeezing microwaves by magnetostriction, Nat. Sci. Rev. **10**, nwac247 (2023).
[13] J. Li and S. Gröblacher, Entangling the vibrational modes of two massive ferromagnetic spheres using cavity magnomechanics, Quantum Sci. Technol. **6**, 024005 (2021).
[14] J. Li and S. Y. Zhu, Entangling two magnon modes via magnetostrictive interaction, New J. Phys. **21**, 085001 (2019).
[15] Z.-X. Liu, J. Peng, and H. Xiong, Generation of magnonic frequency combs via a two-tone microwave drive, Phys. Rev. A **107**, 053708 (2023).
[16] G.-T. Xu, M. Zhang, Y. Wang, Z. Shen, G.-C. Guo, and C.-H. Dong, Magnonic frequency comb in the magnomechanical resonator, Phys. Rev. Lett. **131**, 243601 (2023).
[17] H. Xiong, Magnonic frequency combs based on the resonantly enhanced magnetostrictive effect, Fundam. Res. **3**, 8 (2023).
[18] Z.-X. Liu and Y.-Q. Li, Optomagnonic frequency combs, Photon. Res. **10**, 2786 (2022).
[19] J. Peng, Z.-X. Liu, Y.-F. Yu, and H. Xiong, Cavity magnomechanical chaos, Phys. Rev. A **110**, 053704 (2024).
[20] B. Wang, C. Kong, Z.-X. Liu, H. Xiong, and Y. Wu, Magnetic-field-controlled magnon chaos in an active cavity-magnon system, Laser Phys. Lett. **16**, 045208 (2019).
[21] Z.-X. Liu, C. You, B. Wang, H. Xiong, and Y. Wu, Phase-mediated magnon chaos-order transition in cavity optomagnonics, Opt. Lett. **44**, 507 (2019).
[22] T.-X. Lu, Z.-S. Li, L.-S. Chen, Y. Wang, X. Xiao, and H. Jing, Nonreciprocal entanglement in cavity magnomechanics via the Barnett effect, Phys. Rev. A **111**, 013713 (2025).
[23] Z.-Q. Liu, J. Liu, L. Tan, and W.-M. Liu, Twice-enhanced quantum entanglement in a dual-coupled auxiliary-sphere-assisted cavity magnomechanical system, Phys. Rev. A **110**, 023707 (2024).
[24] Dilawaiz, S. Qamar, and M. Irfan, Entangled atomic ensemble and an yttrium-iron-garnet sphere in coupled microwave cavities, Phys. Rev. A **109**, 043708 (2024).
[25] Y.-C. Ye, Q.-C. Li, T.-L. Yang, and Y.-J. Xu, Phase-controlled quantum entanglement and one-way steering in cavity magnonic system, Opt. Express **32**, 36907 (2024).
[26] B. Hussain, S. Qamar, and M. Irfan, Entanglement enhancement in cavity magnomechanics by an optical parametric amplifier, Phys. Rev. A **105**, 063704 (2022).
[27] W.-J. Wu, Y.-P. Wang, J.-Z. Wu, J. Li, and J. Q. You, Remote magnon entanglement between two massive ferrimagnetic spheres via cavity optomagnonics, Phys. Rev. A **104**, 023711 (2021).
[28] J. Li, S.-Y. Zhu, and G. S. Agarwal, Magnon-photon-phonon entanglement in cavity magnomechanics, Phys. Rev. Lett. **121**, 203601 (2018).
[29] J. Chen, X.-G. Fan, W. Xiong, D. Wang, and L. Ye, Nonreciprocal entanglement in cavity-magnon optomechanics, Phys. Rev. B **108**, 024105 (2023).
[30] J. Chen, M. Rossi, D. Mason, and A. Schliesser, Entanglement of propagating optical modes via a mechanical interface, Nat. Commun. **11**, 943 (2020).
[31] S. Barzanjeh, E. S. Redchenko, M. Peruzzo, M. Wulf, D. P. Lewis, G. Arnold, and J. M. Fink, Stationary entangled radiation from micromechanical motion, Nature (London) **570**, 480 (2019).
[32] L. Mercier de Lépinay, C. F. Ockeloen-Korppi, M. J. Woolley, and M. A. Sillanpää, Quantum mechanics–free subsystem with mechanical oscillators, Science **372**, 625 (2021).
[33] S. Kotler, G. A. Peterson, E. Shojaee, F. Lecocq, K. Cicak, A. Kwiatkowski, S. Geller, S. Glancy, E. Knill, R. W. Simmonds, J. Aumentado, and J. D. Teufel, Direct observation of deterministic macroscopic entanglement, Science **372**, 622 (2021).
[34] C. F. Ockeloen-Korppi, E. Damskägg, J.-M. Pirkkalainen, M. Asjad, A. A. Clerk, F. Massel, M. J. Woolley, and M. A. Sillanpää, Stabilized entanglement of massive mechanical oscillators, Nature (London) **556**, 478 (2018).
[35] R. Riedinger, A. Wallucks, I. Marinković, C. Löschnauer, M. Aspelmeyer, S. Hong, and S. Gröblacher, Remote quantum entanglement between two micromechanical oscillators, Nature (London) **556**, 473 (2018).
[36] Y. Chen, Y.-L. Zhang, Z. Shen, C.-L. Zou, G.-C. Guo, and C.-H. Dong, Synthetic gauge fields in a single optomechanical resonator, Phys. Rev. Lett. **126**, 123603 (2021).
[37] L. Ren, S. Yuan, S. Zhu, L. Shi, and X. Zhang, Backscattering-induced chiral absorption in optical microresonators, ACS Photonics **10**, 3797 (2023).
[38] J. Zhao, L. Wu, T. Li, Y.-X. Liu, F. Nori, Y. Liu, and J. Du, Phase-controlled pathway interferences and switchable fast-slow light in a cavity-magnon polariton system, Phys. Rev. Appl. **15**, 024056 (2021).
[39] X.-B. Yan, H.-L. Lu, F. Gao, and L. Yang, Perfect optical nonreciprocity in a double-cavity optomechanical system, Front. Phys. **14**, 52601 (2019).
[40] X.-W. Xu and Y. Li, Optical nonreciprocity and optomechanical circulator in three-mode optomechanical systems, Phys. Rev. A **91**, 053854 (2015).
[41] X.-Y. Zhang, C. Cao, Y.-P. Gao, L. Fan, R. Zhang, and C. Wang, Generation and manipulation of phonon lasering in a two-drive cavity magnomechanical system, New J. Phys. **25**, 053039 (2023).
[42] F. X. Sun, D. Mao, Y. T. Dai, Z. Ficek, Q. Y. He, and Q. H. Gong, Phase control of entanglement and quantum steering in a three-mode optomechanical system, New J. Phys. **19**, 123039 (2017).

[43] J.-X. Liu, Y.-F. Jiao, Y. Li, X.-W. Xu, Q.-Y. He, and H. Jing, Phase-controlled asymmetric optomechanical entanglement against optical backscattering, Sci. China Phys. Mech. Astron. **66**, 230312 (2023).
[44] J.-X. Liu, J.-Y. Yang, T.-X. Lu, Y.-F. Jiao, and H. Jing, Phase-controlled robust quantum entanglement of remote mechanical oscillators, Phys. Rev. A **109**, 023519 (2024).
[45] M. Li, Y.-L. Zhang, S.-H. Wu, C.-H. Dong, X.-B. Zou, G.-C. Guo, and C.-L. Zou, Single-mode photon blockade enhanced by bi-tone drive, Phys. Rev. Lett. **129**, 043601 (2022).
[46] X.-W. Xu, Y. Li, B. Li, H. Jing, and A.-X. Chen, Nonreciprocity via nonlinearity and synthetic magnetism, Phys. Rev. Appl. **13**, 044070 (2020).
[47] J. Huang and Z. Zhang, Room-temperature exciton-vibrationphoton entanglement in polariton optomechanics, Phys. Rev. A **112**, 013509 (2025).
[48] X.-L. Yin, H. J. Lee, and G. Zhang, Giant-atom dephasing dynamics and entanglement generation in a squeezed vacuum reservoir, Phys. Rev. A **111**, 033707 (2025).
[49] T.-X. Lu, B. Li, Y. Wang, D.-Y. Wang, X. Xiao, and H. Jing, Directional quantum-squeezing-enabled nonreciprocal enhancement of entanglement, Phys. Rev. Appl. **22**, 064001 (2024).
[50] J. Huang, D. Lei, G. S. Agarwal, and Z. Zhang, Collective quantum entanglement in molecular cavity optomechanics, Phys. Rev. B **110**, 184306 (2024).
[51] X.-L. Hei, P.-B. Li, X.-F. Pan, and F. Nori, Enhanced tripartite interactions in spin-magnon-mechanical hybrid systems, Phys. Rev. Lett. **130**, 073602 (2023).
[52] H. Zhou, T. Li, and K. Xia, Parallel and heralded multiqubit entanglement generation for quantum networks, Phys. Rev. A **107**, 022428 (2023).
[53] J. Huang, D.-G. Lai, and J.-Q. Liao, Thermal-noise-resistant optomechanical entanglement via general dark-mode control, Phys. Rev. A **106**, 063506 (2022).
[54] D.-G. Lai, J.-Q. Liao, A. Miranowicz, and F. Nori, Noise-tolerant optomechanical entanglement via synthetic magnetism, Phys. Rev. Lett. **129**, 063602 (2022).
[55] Y.-F. Jiao, J.-X. Liu, Y. Li, R. Yang, L.-M. Kuang, and H. Jing, Nonreciprocal enhancement of remote entanglement between nonidentical mechanical oscillators, Phys. Rev. Appl. **18**, 064008 (2022).
[56] H. Tan and J. Li, Einstein-Podolsky-Rosen entanglement and asymmetric steering between distant macroscopic mechanical and magnonic systems, Phys. Rev. Res. **3**, 013192 (2021).
[57] Y.-F. Jiao, S.-D. Zhang, Y.-L. Zhang, A. Miranowicz, L.-M. Kuang, and H. Jing, Nonreciprocal optomechanical entanglement against backscattering losses, Phys. Rev. Lett. **125**, 143605 (2020).
[58] M. Yu, H. Shen, and J. Li, Magnetostrictively induced stationary entanglement between two microwave fields, Phys. Rev. Lett. **124**, 213604 (2020).
[59] W. Qin, A. Miranowicz, P.-B. Li, X.-Y. Lü, J. Q. You, and F. Nori, Exponentially enhanced light-matter interaction, cooperativities, and steady-state entanglement using parametric amplification, Phys. Rev. Lett. **120**, 093601 (2018).
[60] X.-Y. Lü, G.-L. Zhu, L.-L. Zheng, and Y. Wu, Entanglement and quantum superposition induced by a single photon, Phys. Rev. A **97**, 033807 (2018).
[61] X. Zhang, C.-L. Zou, L. Jiang, and H. X. Tang, Cavity magnomechanics, Sci. Adv. **2**, e1501286 (2016).
[62] J. Nemarich, Contribution of the two-magnon process to magnetostatic-mode relaxation, Phys. Rev. **136**, A1657 (1964).
[63] C. Kittel, On the theory of ferromagnetic resonance absorption, Phys. Rev. **73**, 155 (1948).
[64] J. T. Hou and L. Liu, Strong coupling between microwave photons and nanomagnet magnons, Phys. Rev. Lett. **123**, 107702 (2019).
[65] G.-Q. Zhang, Y.-P. Wang, and J.-Q. You, Theory of the magnon Kerr effect in cavity magnonics, Sci. China Phys. Mech. Astron. **62**, 987511 (2019).
[66] H. Keshtgar, M. Zareyan, and G. E. W. Bauer, Acoustic parametric pumping of spin waves, Solid State Commun. **198**, 30 (2014).
[67] S. Wang and T. L. Hsu, Spin-wave experiments: Parametric excitation of acoustic waves and mode-locking of spin waves, Appl. Phys. Lett. **16**, 111 (1970).
[68] E. G. Spencer and R. C. LeCraw, Magnetoacoustic resonance in yttrium iron garnet, Phys. Rev. Lett. **1**, 241 (1958).
[69] D. Hatanaka, M. Asano, H. Okamoto, Y. Kunihashi, H. Sanada, and H. Yamaguchi, On-chip coherent transduction between magnons and acoustic phonons in cavity magnomechanics, Phys. Rev. Appl. **17**, 034024 (2022).
[70] Z. Shen, G.-T. Xu, M. Zhang, Y.-L. Zhang, Y. Wang, C.-Z. Chai, C.-L. Zou, G.-C. Guo, and C.-H. Dong, Coherent coupling between phonons, magnons, and photons, Phys. Rev. Lett. **129**, 243601 (2022).
[71] J. Qian, J. Li, S.-Y. Zhu, J. Q. You, and Y.-P. Wang, Probing $\mathcal{PT}$-symmetry breaking of non-Hermitian topological photonic states via strong photon-magnon coupling, Phys. Rev. Lett. **132**, 156901 (2024).
[72] R.-C. Shen, J. Li, Z.-Y. Fan, Y.-P. Wang, and J. Q. You, Mechanical bistability in Kerr-modified cavity magnomechanics, Phys. Rev. Lett. **129**, 123601 (2022).
[73] C. W. Gardiner and P. Zoller, *Quantum Noise* (Springer, Berlin, 2000).
[74] A. Rocco and P. Grigolini, The Markov approximation revisited: Inconsistency of the standard quantum Brownian motion model, Phys. Lett. A **252**, 115 (1999).
[75] V. Giovannetti and D. Vitali, Phase-noise measurement in a cavity with a movable mirror undergoing quantum Brownian motion, Phys. Rev. A **63**, 023812 (2001).
[76] D. Vitali, S. Gigan, A. Ferreira, H. R. Böhm, P. Tombesi, A. Guerreiro, V. Vedral, A. Zeilinger, and M. Aspelmeyer, Optomechanical entanglement between a movable mirror and a cavity field, Phys. Rev. Lett. **98**, 030405 (2007).
[77] E. X. DeJesus and C. Kaufman, Routh-Hurwitz criterion in the examination of eigenvalues of a system of nonlinear ordinary differential equations, Phys. Rev. A **35**, 5288 (1987).
[78] G. Adesso, A. Serafini, and F. Illuminati, Extremal entanglement and mixedness in continuous variable systems, Phys. Rev. A **70**, 022318 (2004).
[79] R. Simon, Peres-Horodecki separability criterion for continuous variable systems, Phys. Rev. Lett. **84**, 2726 (2000).
[80] G. Adesso and F. Illuminati, Continuous variable tangle, monogamy inequality, and entanglement sharing in Gaussian states of continuous variable systems, New J. Phys. **8**, 15 (2006).

[81] G. Adesso and F. Illuminati, Entanglement in continuous-variable systems: Recent advances and current perspectives, J. Phys. A: Math. Theor. **40**, 7821 (2007).

[82] V. Coffman, J. Kundu, and W. K. Wootters, Distributed entanglement, Phys. Rev. A **61**, 052306 (2000).

[83] D. Zhang, X.-Q. Luo, Y.-P. Wang, T.-F. Li, and J. Q. You, Observation of the exceptional point in cavity magnon-polaritons, Nat. Commun. **8**, 13687 (2017).

[84] L. Gyongyosi and S. Imre, A survey on quantum computing technology, Comput. Sci. Rev. **31**, 51 (2019).

[85] E. Knill, Quantum computing with realistically noisy devices, Nature (London) **434**, 39 (2005).

[86] J. L. O'Brien, Optical quantum computing, Science **318**, 1567 (2007).

[87] K. A. Gilmore, M. Affolter, R. J. Lewis-Swan, D. Barberena, E. Jordan, A. M. Rey, and J. J. Bollinger, Quantum-enhanced sensing of displacements and electric fields with two-dimensional trapped-ion crystals, Science **373**, 673 (2021).

[88] C. L. Degen, F. Reinhard, and P. Cappellaro, Quantum sensing, Rev. Mod. Phys. **89**, 035002 (2017).

[89] S. Barzanjeh, S. Pirandola, D. Vitali, and J. M. Fink, Microwave quantum illumination using a digital receiver, Sci. Adv. **6**, eabb0451 (2020).

[90] W. Chen, Ş. K. Özdemir, G. Zhao, J. Wiersig, and L. Yang, Exceptional points enhance sensing in an optical microcavity, Nature (London) **548**, 192 (2017).

[91] H. Shen, X. Su, X. Jia, and C. Xie, Quantum communication network utilizing quadripartite entangled states of optical field, Phys. Rev. A **80**, 042320 (2009).

[92] S. L. N. Hermans, M. Pompili, H. K. C. Beukers, S. Baier, J. Borregaard, and R. Hanson, Qubit teleportation between non-neighbouring nodes in a quantum network, Nature (London) **605**, 663 (2022).

[93] C. Simon, Towards a global quantum network, Nat. Photon. **11**, 678 (2017).

[94] P. Kómár, E. M. Kessler, M. Bishof, L. Jiang, A. S. Sørensen, J. Ye, and M. D. Lukin, A quantum network of clocks, Nat. Phys. **10**, 582 (2014).

[95] T.-X. Lu, X. Xiao, L.-S. Chen, Q. Zhang, and H. Jing, Magnon-squeezing-enhanced slow light and second-order sideband in cavity magnomechanics, Phys. Rev. A **107**, 063714 (2023).

[96] T.-X. Lu, H. Zhang, Q. Zhang, and H. Jing, Exceptional-point-engineered cavity magnomechanics, Phys. Rev. A **103**, 063708 (2021).

[97] S.-N. Huai, Y.-L. Liu, J. Zhang, L. Yang, and Y.-X. Liu, Enhanced sideband responses in a $\mathscr{PT}$-symmetric-like cavity magnomechanical system, Phys. Rev. A **99**, 043803 (2019).

[98] W. Zhang, S. Liu, S. Zhang, and H.-F. Wang, Magnon blockade induced by parametric amplification, Phys. Rev. A **109**, 043712 (2024).

[99] Y. Wang, W. Xiong, Z. Xu, G.-Q. Zhang, and J.-Q. You, Dissipation-induced nonreciprocal magnon blockade in a magnon-based hybrid system, Sci. China Phys. Mech. Astron. **65**, 260314 (2022).

[100] C. Zhao, X. Li, S. Chao, R. Peng, C. Li, and L. Zhou, Simultaneous blockade of a photon, phonon, and magnon induced by a two-level atom, Phys. Rev. A **101**, 063838 (2020).

[101] Q. Zhang, J. Wang, T.-X. Lu, R. Huang, F. Nori, and H. Jing, Quantum weak force sensing with squeezed magnomechanics, Sci. China Phys. Mech. Astron. **67**, 100313 (2024).

[102] C. A. Potts, V. A. S. V. Bittencourt, S. V. Kusminskiy, and J. P. Davis, Magnon-phonon quantum correlation thermometry, Phys. Rev. Appl. **13**, 064001 (2020).

[103] M. F. Colombano, G. Arregui, F. Bonell, N. E. Capuj, E. Chavez-Angel, A. Pitanti, S. O. Valenzuela, C. M. Sotomayor-Torres, D. Navarro-Urrios, and M. V. Costache, Ferromagnetic resonance assisted optomechanical magnetometer, Phys. Rev. Lett. **125**, 147201 (2020).